Available online at www.sciencedirect.com
SCIENCE DIRECT®
International Journal of Mass Spectrometry 228 (2003) 865–877
International Journal of Mass Spectrometry
www.elsevier.com/locate/ijms

Bonding interactions in $Ag^+(O_2)_n$ and $Ag_2^+(O_2)_n$ clusters: experiment and theory

Manuel J. Manard, Paul R. Kemper, Michael T. Bowers*

Department of Chemistry & Biochemistry, University of California, Santa Barbara, CA 93106, USA

Received 20 March 2003; accepted 8 April 2003

Dedicated to Prof. Helmut Schwarz on the occasion of his 60th birthday.

Abstract

Equilibrium methods were used to measure binding energies and entropies for the attachment of up to four O_2 ligands to ground-state $Ag^+(^1S, 4d^{10})$ and for the attachment of up to three O_2 ligands to ground-state $Ag_2^+(^2\Sigma_g, 4d^{20}\ \sigma(5s)^1)$. Bond dissociation energies (BDEs) of the first three O_2 ligands from $Ag^+(O_2)_n$ are 6.9, 7.4, and 5.5 kcal/mol for $n = 1$–3, respectively, with the BDE of the fourth ligand estimated to be 4.8 kcal/mol. BDEs of the first and second O_2 ligands from $Ag_2^+(O_2)_n$ are 4.5 and 4.2 kcal/mol, respectively, with the BDE of the third ligand estimated to be 3.5 kcal/mol. All of the observed attachments of O_2 ligands to both the monomer and dimer Ag core ions were within the first solvation shell. Theoretical calculations at the DFT-B3LYP level were done on all of the observed Ag^+ and Ag_2^+ clusters in order to determine the vibrational frequencies and geometries and to examine the origin of the bonding and its variation with core ion coordination. Comparisons are made with the $Cu^+(H_2)_n$ and $Cu_2^+(H_2)_n$ systems.
© 2003 Elsevier B.V. All rights reserved.

Keywords: Bonding interactions; $Ag^+(O_2)_n$ cluster; $Ag_2^+(O_2)_n$ cluster

1. Introduction

From biological systems to industrial processes, transition metals have proven to be essential components of a vast array of catalytic reactions. Despite their widespread usage, many of the details of how transition metals aid these reactions remain essentially unknown. However, over the past 15 years, experiments conducted on gas phase transition metal ion clusters have shed new light on this subject [1–19]. These experiments have broadened our understanding of the nature of transition metal ion bonding from a simple electrostatic view to an awareness of the complex covalent factors that are involved. Many of these experiments have examined the binding between oxidized transition metal core ions with small, uninserted ligands. This was first shown to be possible by the experiments of Kubas et al. [1], where uninserted H_2 molecules were bound to a transition metal center. In the time that has followed, systematic experiments have examined the properties of numerous gas phase metal ion $M^+ - X_n$ [2–19] clusters. Relatively simple systems with $X = H_2$ [2–12], CO [13–18], and methane [3,19] have been examined, along with a variety of other ligands [20,21]. The influence of the electronic structure of the metal ion on both the binding

* Corresponding author. Tel.: +1-805-893-2893; fax: +1-805-893-8703.
E-mail address: bowers@chem.ucsb.edu (M.T. Bowers).

1387-3806/$ – see front matter © 2003 Elsevier B.V. All rights reserved.
doi:10.1016/S1387-3806(03)00245-8

energies and structures of these clusters clearly show the presence of covalent forces in the bonding. The large difference in $M^+ - X_n$ bond energies between the truly inert alkali ions and the transition metals reinforces this observation [22]. Additionally, the relatively small size of these clusters makes them well suited for modeling with high-level ab initio calculations. These calculations have proven necessary to gain a complete understanding of both the structures and the underlying bonding processes present in these systems [20]. The ability to examine these relatively small transition metal clusters in great detail makes them excellent prototype systems for studying the elementary steps of their catalytic processes.

Recently, there has been an increased interest in the bonding interactions of Au and Ag clusters with O_2. This is due to the recent discovery that small Au clusters are good oxidation catalysts [23]. Although theoretical investigations into the binding characteristics of O_2 with Ag and Au clusters, both ionic and neutral, have been conducted in order to determine binding energies, molecular geometries, and other properties [24,25], and some experiments have also been performed to measure binding energies of negative Au clusters with O_2 ligands [26–29], detailed information about these newly discovered catalytic properties of Ag and Au is not yet available. To help elucidate the origin of their catalytic properties, we have initiated a broad-based effort at University of California, Santa Barbara to investigate these properties, both for clusters on metal oxide surfaces and in the gas phase. Our initial studies are reported here where $Ag^+(O_2)_n$ and $Ag_2{}^+(O_2)_n$ clusters were examined using temperature-dependent equilibrium measurements as well as ab initio calculations. Of particular interest is the nature of the interaction of these Ag clusters with O_2 and how these interactions compare with the analogous $Cu^+(H_2)_n$ [11] and $Cu_2{}^+(H_2)_n$ [12] clusters reported earlier. Although the ligands in the Cu and Ag studies differ, the similarities in the valence electronic structures of $Ag^+(4d^{10})$ and $Cu^+(3d^{10})$, and $Ag_2{}^+(4d^{20}\ \sigma(5s)^1)$ and $Cu_2{}^+(3d^{20}\ \sigma(5s)^1)$, should prove interesting as a point of comparison. We present here a combined experimental and theoretical study of $Ag^+(O_2)_n$ and $Ag_2{}^+(O_2)_n$.

2. Experimental

A description of the instrument and experimental details has been given previously [5,7,30], and only a brief description will be given here. The Ag^+ and $Ag_2{}^+$ ions are generated from a translating/rotating silver rod with a pulsed laser vaporization ion source using an Ar bath gas. The preferred isotope (either $^{107}Ag^+$ or $^{109}Ag^+$ for the monomer or $^{214}Ag_2{}^+$, $^{216}Ag_2{}^+$ or $^{218}Ag_2{}^+$ for the dimer) is then mass selected by a quadrupole mass filter and injected into a 4-cm long drift/reaction cell. The cell is typically filled with 1–4 Torr of O_2 gas. Equilibria are quickly established as the various $Ag^+(O_2)_n$ and $Ag_2{}^+(O_2)_n$ clusters are drawn through the cell under the influence of a small electric field. The electric field is small enough so that the thermal energy of the ions is not significantly perturbed. The clusters exiting the cell are then mass selected by a second quadrupole and detected. Peak intensities are recorded and integrated and these values, along with the pressure of O_2 (P_{O_2}) in Torr, are used to determine an equilibrium constant (K_p°) for the reaction from Eq. (1).

$$K_p^\circ = \frac{[Ag_{1,2}{}^+(O_2)_n]}{[Ag_{1,2}(O_2)_{n-1}]} \times \frac{760}{P_{O_2}} \tag{1}$$

The equilibrium constant can then be used to calculate the standard Gibbs free energy of the reaction,

$$\Delta G_T^\circ = -RT \ln[K_p^\circ] \tag{2}$$

and the values obtained for ΔG_T° plotted vs. the temperature, to obtain ΔS_T° and ΔH_T° from Eq. (3)

$$\Delta G_T^\circ = \Delta H_T^\circ - T\,\Delta S_T^\circ \tag{3}$$

The resulting plots are linear over the experimental temperature range and a least squared fitting procedure is used to obtain slopes equal to the association entropy (ΔS_T°) of the reaction and intercepts equal to the binding energy (ΔH_T°) of the molecule. The reported uncertainty in these values is a measure of variance in

the data from the fit. ΔH_0° is then determined by fitting and extrapolating the data to 0 K using statistical thermodynamics. The necessary vibrational frequencies and rotational constants are taken from density functional theory (DFT) [31] calculations (see next section). In all cases, vibrational frequencies are varied over a wide range, and the effect on ΔH_0° is included in the error limits. It should be stressed that uncertainties in these parameters have little effect on the final values of ΔH_0°. For a thorough discussion of this fitting procedure and an estimation of the errors involved, see Refs. [2] and [5]. The bond dissociation energy (BDE) is equal to $-\Delta H_0^\circ$.

3. Theory

The product ions discussed here were all examined theoretically to determine the molecular parameters needed to analyze the experimental data and to identify factors important in the bonding. Calculations were carried out at the DFT level using the B3LYP hybrid functional [32,33], using the Gaussian 98 package [34]. For all of the calculations performed in this work, oxygen was described using the standard 6-311+G* basis set [35]. The basis set for silver is a (5s6p4d)/[3s3p2d] contraction of the Hay–Wadt $(n+1)$ effective core potential (ECP) valence double zeta basis proposed by Hay and Wadt [36].[1] Here, the outermost core orbitals are not replaced by the ECP, but are instead treated equally with the valence orbitals. This allows for increased accuracy in the calculations without a substantial increase in computation time. The ECP for silver incorporates the Darwin and mass–velocity relativistic effects into the potential.

[1] Basis sets were obtained from the Extensible Computational Chemistry Environment Basis Set Database, Version 10/29/02, as developed and distributed by the Molecular Science Computing Facility, Environmental and Molecular Sciences Laboratory which is part of the Pacific Northwest Laboratory, P.O. Box 999, Richland, Washington 99352, USA, and funded by the U.S. Department of Energy. The Pacific Northwest Laboratory is a multi-program laboratory operated by Battelle Memorial Institute for the U.S. Department of Energy under contract DE-AC06-76RLO 1830. Contact David Feller or Karen Schuchardt for further information.

Geometry optimizations of $Ag^+(O_2)_n$ and $Ag_2^+(O_2)_n$ clusters were performed over a wide range of geometries in order to determine a true global minimum. All confirmed minima consist of largely unperturbed O_2 ligands bound to a transition metal core ion. Vibrational frequencies were calculated for all minima. All reported vibrational frequencies are unscaled.

4. Results and discussion

A summary of the experimental enthalpies and entropies as well as theoretical binding energies for the reaction $Ag^+(O_2)_{n-1} + O_2 \rightleftarrows Ag^+(O_2)_n$ is given in Table 1. The corresponding calculated vibrational frequencies are listed in Table 2. Experimental enthalpies, entropies, and theoretical binding energies for the reaction $Ag_2^+(O_2)_{n-1} + O_2 \rightleftarrows Ag_2^+(O_2)_n$ are given in Table 3 and the corresponding calculated vibrational frequencies are listed in Table 4. All of the cluster ions discussed here consist either of an intact Ag^+ or Ag_2^+ core ion surrounded by largely unperturbed O_2 ligands. No evidence of insertion to form a dioxide was found.

5. $Ag^+(O_2)_n$ clusters

5.1. $Ag^+(O_2)$

The experimental ΔH_T° and ΔS_T° values for dissociation of $Ag^+(O_2)$ are -7.1 kcal/mol and -15.0 cal/(mol K), respectively (Table 1). Fig. 1 shows both the experimental free energy and that calculated from statistical mechanics using theoretically determined vibrational frequencies (Table 2) and rotational constants. The resulting experimental BDE $(-\Delta H_0^\circ)$ of $Ag^+(O_2)$ is 6.9 kcal/mol, in good agreement with the calculated (DFT) binding energy (D_o) of 6.30 kcal/mol. The first O_2 ligand adds in a bent triatomic conformation to Ag^+ (Fig. 2). The calculated Ag^+–O_2 bond distance is 2.466 Å with an associated O–O bond length of 1.204 Å, shorter than the theoretical O–O bond distance of 1.206 Å calculated for free O_2. The Ag–O–O angle of $Ag^+(O_2)$ is 137.5°.

Table 1
Data summary for $Ag^+(O_2)_{n-1} + O_2 \rightleftarrows Ag^+(O_2)_n$

Experiment					Theory	
n	$-\Delta H_T^\circ$ [a]	$-\Delta S_T^\circ$ [b]	$-\Delta H_0^\circ$ [c]	T [d]	D_e [a]	D_o [a]
1	7.1 ± 0.2	15.0 ± 1	6.9 ± 0.3	310 ± 75	6.66	6.30
2	7.6 ± 0.2	21.4 ± 1	7.4 ± 0.3	220 ± 40	7.11	6.47
3	5.7 ± 0.2	19.3 ± 2	5.5 ± 0.3	160 ± 20	4.58	4.24
4			4.8[e]	140	4.16	3.91

[a] In units of kcal/mol.
[b] In units of cal/(mol K).
[c] Value from fitting data with theoretical vibrational frequencies, rotational constants and geometries, in units of kcal/mol.
[d] In Kelvin, ± refers to the experimental temperature range not uncertainty.
[e] Estimate, assuming the same ΔS_T° as $n = 3$ (see text).

Table 2
Theoretical vibrational frequencies for $Ag^+(O_2)_n$ clusters[a,b]

	O–O stretch	Ag^+–O_2 symmetric stretch	Ag^+–O_2 asymmetric stretch	O_2–Ag^+–O_2 bends and torsions
$Ag^+(O_2)$	1622	177		87
$Ag^+(O_2)_2$	1622(2)	175	204	25[c], 60, 62, 94, 111
$Ag^+(O_2)_3$	1625(2), 1626	154	159, 169	17[c], 23[c], 28[c], 31, 34, 52, 82, 85, 90
$Ag^+(O_2)_4$	1626, 1627(3)	144	142, 143, 150	8[c], 13, 15[c], 17[c], 19, 25[c], 33, 39, 40, 73(2), 79, 82
O_2	1633			

[a] Harmonic vibrational frequencies for the different $Ag^+(O_2)_n$ clusters as obtained by analytical differentiation of the SCF energy at SCF geometry.
[b] All numbers in cm^{-1}.
[c] Free rotations.

The bonding characteristics of $Ag^+(O_2)$ set trends that are closely followed in the larger $Ag^+(O_2)_n$ clusters. Although the bond strengths in these clusters are relatively weak, never exceeding 7.4 kcal/mol, there is evidence that the bonding interaction between Ag^+ and O_2 is covalent rather than purely electrostatic. Calculations show that about 0.1 electron is donated to Ag^+ in $Ag^+(O_2)$. Upon bonding with Ag^+, a partial negative charge is found on the O atom closest to the transition metal ion, while a partial positive charge is found on the other O atom. This positive charge is slightly greater in magnitude than that of the negative

Table 3
Data summary for $Ag_2^+(O_2)_{n-1} + O_2 \rightleftarrows Ag_2^+(O_2)_n$

Experiment					Theory	
n	$-\Delta H_T^\circ$ [a]	$-\Delta S_T^\circ$ [b]	$-\Delta H_0^\circ$ [c]	T [d]	D_e [a]	D_o [a]
1	4.9 ± 0.4	16.5 ± 2	4.5 ± 0.5	175 ± 25	4.20	3.78
2	4.5 ± 0.3	16.0 ± 3	4.2 ± 0.4	135 ± 15	3.56	3.16
3			3.5[e]	120	2.03	1.76

[a] In units of kcal/mol.
[b] In units of cal/(mol K).
[c] Value from fitting data with theoretical vibrational frequencies, rotational constants and geometries, in units of kcal/mol.
[d] In Kelvin, ± refers to the experimental temperature range not uncertainty.
[e] Estimate, assuming the same ΔS_T° as $n = 2$ (see text).

Table 4
Theoretical vibrational frequencies for $Ag_2^+(O_2)_n$ clusters[a,b]

	Ag–Ag symmetric stretch	O–O stretch	Ag_2^+–O_2 symmetric stretch	Ag_2^+–O_2 asymmetric stretch	O_2–Ag_2^+–O_2 bends and torsions
$Ag_2^+(O_2)$	116	1629	152		30, 53, 73
$Ag_2^+(O_2)_2$	109	1630(2)	152	124	20[d], 29, 30, 50, 55, 73, 66
$Ag_2^+(O_2)_3$	107	1629, 1630[c], 1631[c]	142	98, 113	15, 16[d], 24(2)[d], 27, 33, 35, 46, 49, 59, 65
Ag_2^+	124				
O_2		1633			

[a] Harmonic vibrational frequencies for the different $Ag_2^+(O_2)_n$ clusters as obtained by analytical differentiation of the SCF energy at SCF geometry.
[b] All number in cm^{-1}.
[c] Angled O_2 pair.
[d] Free rotations.

charge on the O atom directly bonded to Ag^+. In other words, the positive charge of Ag^+ induces a dipole moment on the O_2 ligand in which electron density is drawn toward Ag^+. The reduced positive charge of Ag^+ along with the net partial positive charge of the O_2 ligand indicates that electron density is indeed shared between Ag^+ and O_2, which is, by definition, a covalent bond. The charge distribution is given in Fig. 2.

The Ag^+ ion has a $4d^{10}$ $5s^0$ valence configuration, which suggests that the majority of charge donation to Ag^+ is to the unoccupied 5s orbital since the 4d orbitals are fully occupied and the 5p orbitals lie much higher in energy than the 5s orbital. This would be quite similar to the bonding interactions of $Cu^+(H_2)$ [11], where most of the charge transfer from the H_2 ligand is to the unoccupied 4s orbital of Cu^+. The ground-state of O_2 is a triplet, with two unpaired

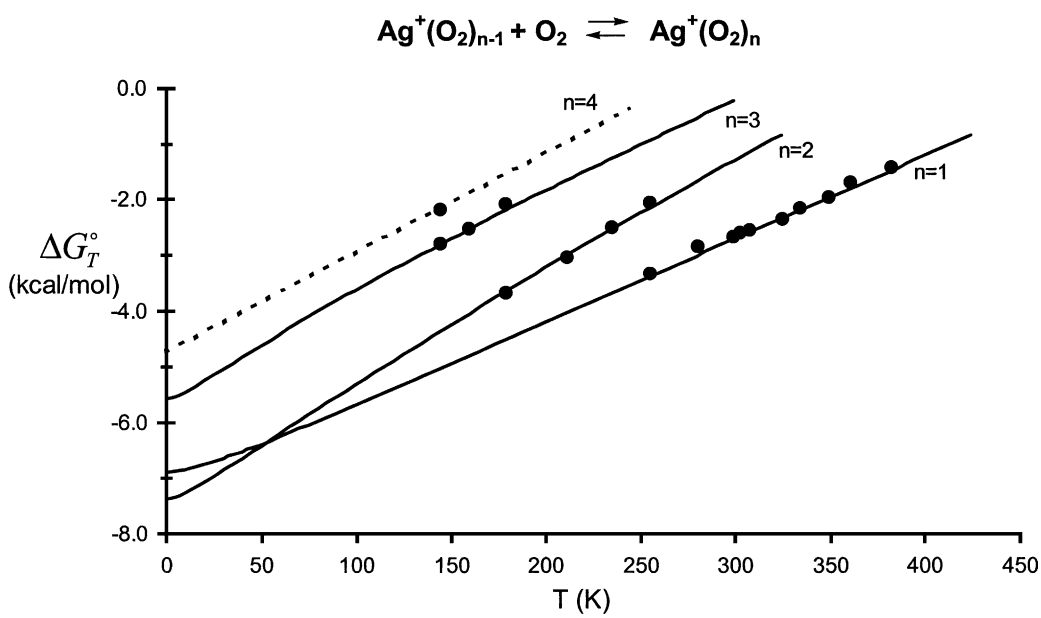

Fig. 1. Plot of experimental ΔG_T° vs. temperature for the association reactions $Ag^+(O_2)_{n-1} + O_2 \rightleftharpoons Ag^+(O_2)_n$. Lines are statistical mechanical fits to the data, which yield values of ΔH_0° at $T = 0$ K.

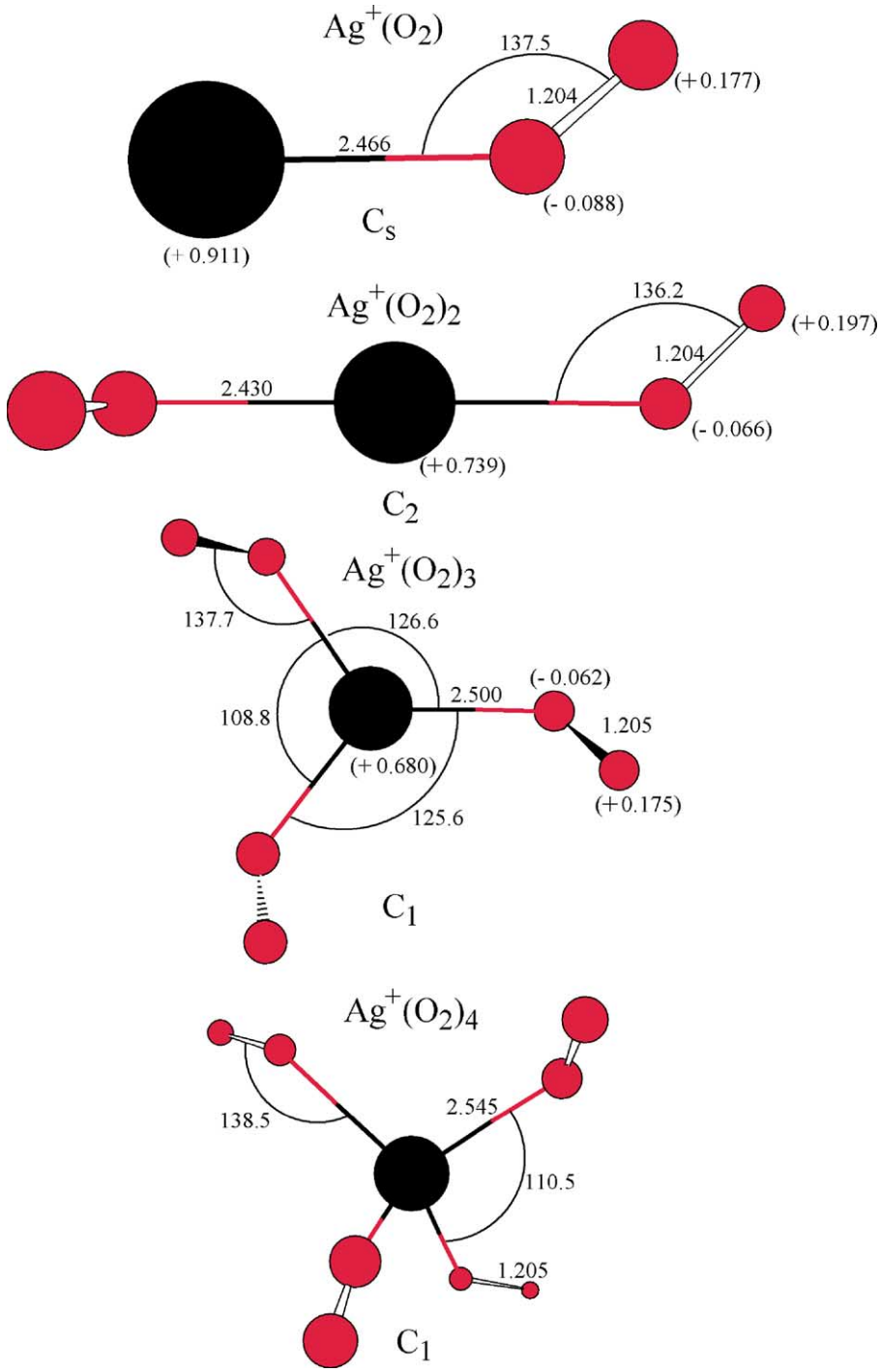

Fig. 2. Theoretical geometries of the $Ag^+(O_2)_n$ clusters calculated at the DFT B3-LYP level. All distances are in angstroms and all angles are in degrees. Partial atomic charges are shown in parentheses. The *z*-axis is taken as the Ag^+–O_2 bonding axis.

electrons in degenerate $\pi^*(2p_x, 2p_y)$ antibonding orbitals. This suggests that donation to Ag^+ should originate from one of the $\pi^*(2p_{x,y})$ orbitals of O_2. NBO population analysis [37] supports this hypothesis. Calculations show that the dominant bond interaction is indeed donation from $\pi^*(2p_{x,y})$ orbital of O_2 to the 5s orbital of Ag^+. This is supported by the relatively weak binding energy of the cluster. Since it is well known that O_2 is a better electron acceptor than donor, electron donation from the $\pi^*(2p_{x,y})$ orbital of O_2 is no doubt an unfavorable process which gives rise to the overall weak bonding interaction of $Ag^+(O_2)$. NBO populations also show that the majority of the electron density present in the 5s orbital of Ag^+ has α spin. This would be expected if donation was from a singly occupied $\pi^*(2p_{x,y})$ orbital. The calculations also indicate that some hybridization between the $4d_{x^2-y^2}$ and 5s orbitals of Ag^+ occurs in order to reduce on-axis Pauli repulsion. This is a minor effect, however.

The suggested bonding scheme of $Ag^+(O_2)$ is supported by the molecular geometry of the cluster. The 137.5° bond angle of $Ag^+(O_2)$ indicates that electron donation must originate from the $\pi^*(2p_{x,y})$ orbitals of O_2. Also, the calculated O–O bond distance of $Ag^+(O_2)$ is slightly reduced compared to that of free O_2 (1.2043 Å as compared to 1.2058 Å, respectively). This is expected since loss of repulsive antibonding electron density should decrease the O–O bond distance in the bound O_2 ligand.

A secondary bonding interaction is also present in the cluster. Specifically, electron density is polarized into the $\sigma^*(2p_z)$ orbital of O_2. The NBO calculation shows increased electron density in the $2p_z$ orbitals of bound O_2 compared to free O_2. Given that the $\sigma(2p_z)$ orbital of O_2 is fully occupied, the increased electron density in these orbitals must be in the $\sigma^*(2p_z)$ orbital. The electron density present in the $\sigma^*(2p_z)$ orbital of O_2 experiences an attractive electrostatic force to Ag^+, which influences the geometry of the cluster. This can be observed by noting the fluctuations in the Ag^+–O–O bond angle in $Ag^+(O_2)_n$ clusters where the $5s/\pi^*(2p_{x,y})$ interaction is relatively strong compared to those where the interaction is weak. A stronger $5s/\pi^*(2p_{x,y})$ interaction gives rise to bond angles nearer 135°. From electron density contour plots of the π^* orbital of O_2, this is what would be expected from a "pure" $\pi^*(2p_{x,y})$ interaction [38]. As the $5s/\pi^*(2p_{x,y})$ interaction weakens, Ag^+–O_2 bond distances increase and Ag^+–O–O bond angles increase. The latter event cannot be attributed to loss of $\pi^*(2p_{x,y})$ donation alone. Instead, it is a combination of decreased $\pi^*(2p_{x,y})$ donation coupled with an electrostatic attraction between Ag^+ and the electron density polarized into the $\sigma^*(2p_z)$ orbital of O_2. This electrostatic interaction causes Ag^+–O–O bond angles to "open" as covalent $\pi^*(2p_{x,y})$ interactions diminish. This interaction is minor in comparison to the $\pi^*(2p_{x,y})$ donation. The NBO calculation shows that the amount of electron density in the $\sigma^*(2p_z)$ orbital of O_2 is essentially the same for all of the clusters that were examined here in both the Ag^+ and Ag_2^+ systems. This lack of change in electron density in the $\sigma^*(2p_z)$ orbital for the larger clusters suggests that the interaction between the $\sigma^*(2p_z)$ on O_2 and the Ag^+ ion is purely electrostatic and that the electron density in the $\sigma^*(2p_z)$ orbital is not due to back donation from 4d orbitals on Ag^+.

5.2. $Ag^+(O_2)_2$

The second O_2 ligand adds opposite the first as shown in Fig. 2 (C_2 symmetry). The experimental ΔH_T° and ΔS_T° values for loss of O_2 from $Ag^+(O_2)_2$ are −7.6 kcal/mol and −21.4 cal/(mol K), respectively. The BDE of $Ag^+(O_2)_2$ was determined by fitting experimental and theoretical ΔG_T° vs. temperature curves and found to be 7.4 kcal/mol, up from 6.9 kcal/mol in the first cluster. The calculated (DFT) binding energy (D_o) for the second cluster is 6.47 kcal/mol, somewhat larger than the 6.30 kcal/mol value calculated for the first O_2 ligand. The theoretical vibrational frequencies for $Ag^+(O_2)_2$ are given in Table 2. The calculated Ag^+–O_2 bond distances are 2.430 Å with associated O–O bond distances of 1.204 Å. The angle produced by an O_2 ligand and Ag^+ is 136.2°. Two alternative *cis*- and *trans*-planar conformations for $Ag^+(O_2)_2$ were found to have theoretical binding energies that are essentially degenerate with the C_2 conformation, differing from one another

by only a few hundredths of kcal/mol. A transition state structure was then calculated in which one O_2 ligand was rotated approximately 45° out of plane in order to determine the rotational barrier between the $Ag^+(O_2)_2$ structures. The rotation barrier was found to approximately 0.1 kcal/mol. This approximate barrier height is well below the thermal energy available, indicating essentially free internal rotation in the system. Such free rotations are not uncommon and have been observed in other transition metal systems [12].

The bonding interactions in $Ag^+(O_2)_2$ are fundamentally the same as those in $Ag^+(O_2)$, with O_2 $\pi^*(2p_{x,y})$ donation to the 5s orbital of Ag^+ and a charge-induced dipole moment causing electron density of the O_2 ligands to be polarized toward Ag^+. This can be seen by the partial negative charges on those O atoms of both O_2 ligands that are directly bonded to Ag^+, and by the net loss of positive charge on Ag^+. As with the first cluster, the electron density polarized into the $\sigma^*(2p_z)$ orbitals of both O_2 ligands plays a minor role in the bonding of $Ag^+(O_2)_2$, via an electrostatic attraction to the Ag^+ core ion. NBO population analysis shows that the populations of the $\sigma^*(2p_z)$ orbitals of the O_2 ligands are essentially the same and are similar to that of the $\sigma^*(2p_z)$ orbital of the O_2 ligand of $Ag^+(O_2)$, providing support for the argument that this interaction is purely electrostatic.

The BDE of the second O_2 ligand in $Ag^+(O_2)_2$ is slightly larger than that of the first cluster. This effect is found for most other transition metal ions binding simple ligands, including the $Cu^+(H_2)_{1,2}$ system. The effect arises from the hybridization of occupied d orbitals with the unoccupied s orbital that occurs when the first ligand binds. This hybridization reduces on-axis Pauli repulsion and is necessarily symmetric. When the second ligand binds, the cost of the hybridization has been paid by the first ligand, producing a larger BDE for the second ligand. In the present case, calculations show that in $Ag^+(O_2)$ and $Ag^+(O_2)_2$ a small amount of electron density is removed from the $4d_{x^2-y^2}$ orbital and promoted into the 5s orbital of Ag^+. The price of this hybridization is paid by the first O_2 ligand, giving rise to the slightly larger second cluster BDE.

The effect of a larger BDE can be seen in the cluster geometry of $Ag^+(O_2)_2$. The Ag^+–O_2 bond lengths and angles of $Ag^+(O_2)_2$ are slightly reduced relative to the analogous features in $Ag^+(O_2)$, suggesting a stronger $\pi^*(2p_{x,y})$/5s interaction. The O–O bond lengths of $Ag^+(O_2)_2$ remain largely unchanged from those of $Ag^+(O_2)$ however, indicating that the increase in the interaction is small. The larger value of ΔS_T° found in the second O_2 association reaction (relative to the first), is mostly due to the loss of two rotational modes that occurs when $Ag^+(O_2)$ reacts with O_2 to form $Ag^+(O_2)_2$. When the atomic ion Ag^+ reacts with O_2 to form $Ag^+(O_2)$, rotational entropy increases giving a less negative ΔS_T° for the first association.

5.3. $Ag^+(O_2)_3$ and $Ag^+(O_2)_4$

Equilibrium for the $Ag^+(O_2)_3$ cluster could only be observed over a very limited temperature range (140–180 K). The experimental ΔH_T° and ΔS_T° values for $Ag^+(O_2)_3$ are −5.7 kcal/mol and −19.3 cal/(mol K), respectively. The BDE of $Ag^+(O_2)_3$ was determined by the usual fitting of experimental ΔG_T° vs. T plots and found to be 5.5 kcal/mol. The calculated (DFT) binding energy (D_o) of $Ag^+(O_2)_3$ is 4.24 kcal/mol, again in reasonable agreement with experiment. It is of interest to note that theory predicts the observed reduction in BDE between the second and third clusters of approximately 2 kcal/mol. Theoretical vibration frequencies for $Ag^+(O_2)_3$ are listed in Table 2. The calculated molecular geometry of $Ag^+(O_2)_3$ is shown in Fig. 2. The calculated Ag^+–O_2 bond distances are 2.500 Å with an associated O–O bond distance of 1.205 Å. The Ag^+–O–O bond angles of $Ag^+(O_2)_3$ are approximately 137.7°. The inner O atoms (those directly bound to Ag^+) and Ag^+ lie in the same plane. The outer O atoms are rotated a few degrees out from this plane, giving rise to a cluster geometry that is nonplanar.

The bonding of $Ag^+(O_2)_3$ is similar to that seen in previous clusters with donation to the 5s orbital of Ag^+ from the $\pi^*(2p_{x,y})$ orbitals of the O_2 ligands as the primary bonding interaction. Again, an electrostatic

interaction between the $\sigma^*(2p_z)$ orbitals of the O_2 ligands and Ag^+ plays a minor role in the bonding of the cluster. Charge-induced dipole moments are once again found on the O_2 ligands, causing electron density to be polarized toward the Ag^+ and eventually, transferred into unoccupied 5s orbital of the transition metal core ion.

The reduced BDE of $Ag^+(O_2)_3$ can be attributed to a reduction in the covalent interaction of the cluster. NBO population analysis indicates similar amounts of electron density in the 5s orbital of Ag^+ for both the $Ag^+(O_2)_2$ and $Ag^+(O_2)_3$ clusters. Since the three O_2 ligands of $Ag^+(O_2)_3$ are donating similar amounts of $\pi^*(2p_{x,y})$ electron density as the two O_2 ligands of $Ag^+(O_2)_2$, it is clear that the average covalent bonding in the third cluster is weaker than that in the second. This reduced covalent interaction is also indicated by the increased Ag^+–O_2 bond distances in the third cluster.

Data for $Ag^+(O_2)_4$ was only taken at 140 K. A BDE of 4.8 kcal/mol for $Ag^+(O_2)_4$ was estimated by assuming an association entropy equal to that of the third cluster. The DFT optimized structure for $Ag^+(O_2)_4$ is shown in Fig. 2. The theoretical binding energy (D_o) for $Ag^+(O_2)_4$ is 3.9 kcal/mol slightly lower than the 4.2 kcal/mol calculated for the third association. The calculated geometry of the fourth cluster is quasi-tetrahedral and shows evidence of a further reduction of covalent interaction in that the Ag^+–O_2 bond distances increase from 2.500 to 2.545 Å as the fourth O_2 ligand is added.

6. $Ag_2^+(O_2)_n$ clusters

6.1. $Ag_2^+(O_2)$

The experimental ΔH_T° and ΔS_T° values for the association of O_2 with Ag_2^+ are −4.9 kcal/mol and −16.5 cal/(mol K), respectively. The BDE of $Ag_2^+(O_2)$ was determined by fitting experimental ΔG_T° vs. T plots (Fig. 3) and found to be 4.5 kcal/mol. Calculations find that the first O_2 ligand binds in a bent configuration to Ag_2^+ in C_s symmetry (Fig. 4). The calculated (DFT) binding energy (D_o) of $Ag_2^+(O_2)$ is 3.78 kcal/mol. As with the $Ag^+(O_2)_n$ clusters, theory

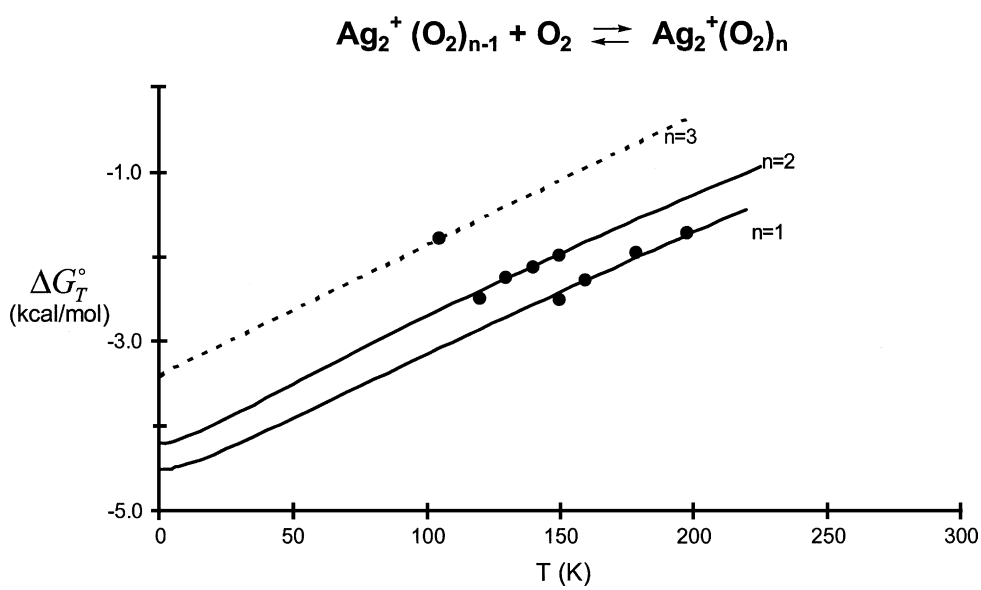

Fig. 3. Plot of experimental ΔG_T° vs. temperature for the association reactions $Ag_2^+(O_2)_{n-1} + O_2 \rightleftarrows Ag_2^+(O_2)_n$. Lines are statistical mechanical fits to the data, which yield values of ΔH_0° at $T = 0$ K.

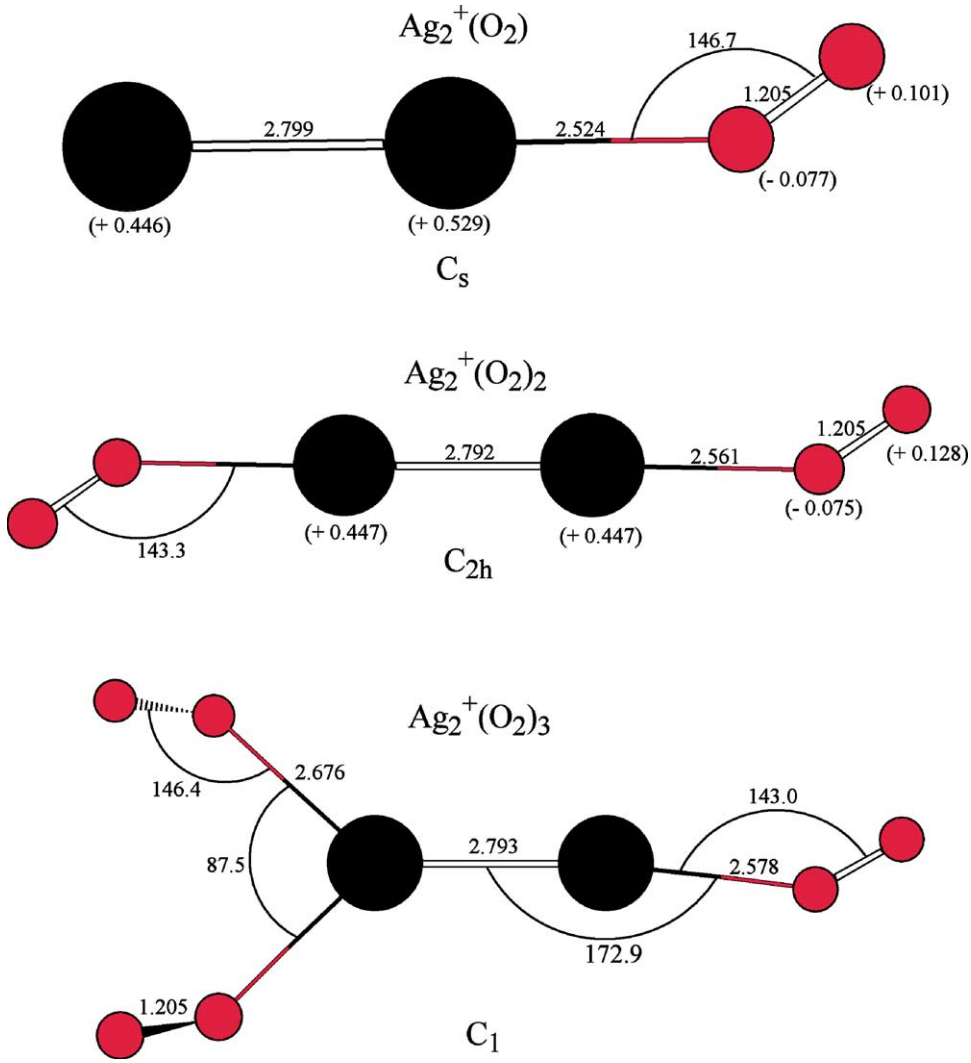

Fig. 4. Theoretical geometries of the $Ag_2^+(O_2)_n$ clusters calculated at the DFT B3-LYP level. All distances are in angstroms and all angles are in degrees. Partial atomic charges are shown in parentheses. The *z*-axis is taken as the Ag_2^+–O_2 bonding axis.

continues to agree well with experiment. Theoretical vibrational frequencies for $Ag_2^+(O_2)$ are listed in Table 4. The calculated Ag_2^+–O_2 bond distance is 2.524 Å with an associated O–O bond distance of 1.205 Å. The Ag_2^+–O–O bond angle is 146.7°.

Bonding in $Ag_2^+(O_2)$ mimics aspects of the bonding in both the $Ag^+(O_2)$ and $Cu_2^+(H_2)$ clusters [12]. The main bonding interactions in $Ag_2^+(O_2)$ remain largely unchanged from the momomer system. The O_2 ligand adds to Ag_2^+ in a "bent-triatomic" conformation indicating the presence of a weak covalent bond formed between Ag_2^+ and O_2 via $\pi^*(2p_{x,y})$ donation from O_2 to the $\sigma(5s)$ orbital of Ag_2^+. This is nearly identical to the bonding interaction in $Ag^+(O_2)$. As with $Ag^+(O_2)$, a charge-induced dipole moment causes O_2 electron density to be polarized toward Ag_2^+. The charges on the various atoms are shown in Fig. 4. Furthermore, electron density polarized into the $\sigma^*(2p_z)$ orbital of O_2 again plays a role in the bonding of the cluster by interacting electrostaticaly

with the Ag_2^+ ion. Here again, NBO population analysis indicates that the amount of electron density in the $\sigma^*(2p_z)$ orbital is essentially the same as that calculated for the $Ag^+(O_2)_n$ clusters.

Although $Ag_2^+(O_2)$ and $Ag^+(O_2)$ share similar bonding traits, some differences between the two clusters do exist and are similar to the differences found between the $Cu_2^+(H_2)$ and $Cu^+(H_2)$ clusters. In the $Ag_2^+(O_2)$ case we find (1) reduced BDEs when compared to that of the analogous momomer cluster (4.5–6.9 kcal/mol), (2) increased transition metal core ion–ligand bond distances and angles, and (3) O–O bond distances closer to those of free O_2. All of these points can be attributed to a reduction of $\pi^*(2p_{x,y})$ donation into the $\sigma(5s)$ orbital of Ag_2^+. As with Cu_2^+, this reduction is caused by the single electron occupation of the σ orbital that forms the bond between $Ag(4d^{10}\ 5s^1)$ and $Ag^+(4d^{10}\ 5s^0)$. The presence of this electron density in the $\sigma(5s)$ orbital of Ag_2^+ increases on-axis Pauli repulsion and serves to destabilize the Ag_2^+–O_2 bond when compared to $Ag^+(O_2)$. Calculations show that the $\sigma(5s)$ electron density of Ag_2^+ is polarized away from the O_2 ligand. This is analogous to what was found in the singly occupied $\sigma(4s)$ orbital of Cu_2^+. The cost of polarizing electron density away from the O_2 ligand as well as increased on-axis Pauli repulsion and reduced donation to Ag_2^+ gives rise to the reduced bond strength in $Ag_2^+(O_2)$.

6.2. $Ag_2^+(O_2)_2$ and $Ag_2^+(O_2)_3$

The experimental ΔH_T° and ΔS_T° values for the formation of $Ag_2^+(O_2)_2$ are -4.5 kcal/mol and -16.0 cal/(mol K), respectively. The BDE of $Ag_2^+(O_2)_2$ was determined by the usual analysis of experimental ΔG_T° vs. T curves and was found to be 4.2 kcal/mol. The calculated (DFT) binding energy (D_o) of $Ag_2^+(O_2)_2$ is 3.16 kcal/mol. Again, reasonable agreement between experiment and theory was obtained. The second O_2 ligand adds opposite the first in C_{2h} symmetry (Fig. 4). The calculated Ag^+–O bond distance is 2.561 Å with an associated O–O bond length of 1.205 Å. The Ag_2^+–O–O bond angle is approximately 143.3°. Theoretical vibrational frequencies for $Ag_2^+(O_2)_2$ are given in Table 4. As with $Ag^+(O_2)_2$, alternative minimum energy conformers exist for $Ag_2^+(O_2)_2$, which are degenerate within the accuracy of the calculation. The first is in C_{2v} symmetry (*cis*) and the second is in C_2 symmetry, with one of the O_2 ligands rotated 90° out of plane with respect to the other. A transition state structure was calculated in which one O_2 ligand was rotated approximately 45° out of plane. The barrier height was found to be approximately 0.08 kcal/mol, indicating essentially free internal rotation in the system (as in the $Ag^+(O_2)_2$ cluster).

The bonding interactions of $Ag_2^+(O_2)_2$ are essentially unchanged from $Ag_2^+(O_2)$, dominated by $\pi^*(2p_{x,y})$ donation from the O_2 ligands to the $\sigma(5s)$ orbital of Ag_2^+ and supplemented by an electrostatic interaction of the $\sigma^*(2p_z)$ orbital of the O_2 ligands with Ag_2^+. As with the other clusters discussed in this work, the core ion charge causes the electron density of the O_2 ligands to be polarized toward the Ag_2^+ core.

Although the bonding of $Ag_2^+(O_2)_2$ is quite similar to $Ag_2^+(O_2)$, the measured BDE of the former cluster is slightly reduced with respect to the latter. This result is unlike the Ag^+ clusters, where the second O_2 ligand binds more strongly than the first because the energy cost of $4d_{x^2-y^2}/5s$ orbital hybridization of Ag^+ is paid upon the first O_2 addition. This increase in BDE does not occur in $Ag_2^+(O_2)_2$ due to the single occupation of the $\sigma(5s)$ orbital of Ag_2^+. Here, much like the singly occupied $\sigma(4s)$ orbital of $Cu_2^+(H_2)_2$, repulsive $\sigma(5s)$ electron density is initially polarized away from the first O_2 ligand. Consequentially, addition of the second ligand must now occur in an area of relatively high electron density. In order to reduce the amount of on-axis repulsion experienced by the second ligand, $\sigma(5s)$ electron density is "repolarized" to near its original distribution in the bare Ag_2^+ core ion. The effect of this process is a decrease in the overall bond strength of $Ag_2^+(O_2)_2$.

A single data point for $Ag_2^+(O_2)_3$ formation was taken at 120 K. This data point was matched with the entropy of the Ag_2^+ second cluster in order to estimate a BDE of 3.5 kcal/mol for $Ag_2^+(O_2)_3$. The DFT

optimized structure for $Ag_2^+(O_2)_3$ is shown in Fig. 4. The theoretical binding energy (D_o) for $Ag_2^+(O_2)_3$ is 1.76 kcal/mol, in reasonable agreement with the estimated experimental value. The theoretical structure of $Ag_2^+(O_2)_3$ (Fig. 4) shows that the addition of the third O_2 ligand is to one of the Ag atoms in Ag_2^+, causing the previously bound ligand to shift approximately 87.5° from the newly bound O_2. Several factors, including reduced electron donation to Ag_2^+, increased σ(5s) repulsion, and ligand–ligand repulsion combine to cause the reduction in bond strength of $Ag_2^+(O_2)_3$.

7. Conclusions

1. Bond dissociation energies and association entropies were determined for $Ag^+(O_2)_{1–4}$ and $Ag_2^+(O_2)_{1–3}$. The Ag^+ BDEs are (in order of cluster size) 6.9, 7.4, 5.5, and ∼4.8 kcal/mol. The Ag_2^+ BDEs are (in order of cluster size) 4.5, 4.2, and ∼3.5 kcal/mol.
2. Density functional theory calculations (B3-LYP parameterization) were done on all the ions to obtain theoretical BDEs, geometries, rotational constants, and vibrational frequencies. Agreement between the theoretical and experimental BDEs is in all cases good, with experimental trends being reproduced by theory although the theoretical BDEs are systematically too small by 0.5–1.0 kcal/mol.
3. Bonding in the clusters consists mainly of electron donation to Ag^+ and Ag_2^+ from the O_2 $\pi^*(2p_{x,y})$ orbital, combined with a minor electrostatic interaction between the $\sigma^*(2p_z)$ orbital of O_2 with the Ag^+ and Ag_2^+ ions, respectively. In all cases, charge induced dipole moments on the O_2 ligands were found to play a role in the bonding of the clusters.
4. The bonding interactions in the $Ag^+(O_2)_n$ and $Ag_2^+(O_2)_n$ cluster ions resembled those in the $Cu^+(H_2)_n$ and the $Cu_2^+(H_2)_n$ systems, respectively. This is not unexpected since the valence shell electron configurations of the $Ag^+(4d^{10})$ and $Ag_2^+(4d^{20}\ \sigma(5s)^1)$ ions are directly analogous to the $Cu^+(3d^{10})$ and $Cu_2^+(3d^{20}\ \sigma(4s)^1)$ ions.

Acknowledgements

The support of the Air Force Office of Scientific Research under grants F 49620-01-1-0459 and F 49620-03-1-0046 are gratefully acknowledged.

References

[1] B.J. Kubas, F.F. Ryan, B.I. Swanson, P.J. Vergamini, H.J. Wasserman, J. Am. Chem. Soc. 106 (1984) 451.
[2] P.R. Kemper, J.E. Bushnell, G. von Helden, M.T. Bowers, J. Phys. Chem. 97 (1993) 52.
[3] P.R. Kemper, J. Bushnell, P.A.M. van Koppen, M.T. Bowers, J. Phys. Chem. 97 (1993) 1810.
[4] J.E. Bushnell, P.R. Kemper, M.T. Bowers, J. Phys. Chem. 97 (1993) 11628.
[5] P.R. Kemper, J. Bushnell, P. Maitre, M.T. Bowers, J. Am. Chem. Soc. 116 (1994) 9710.
[6] J.E. Bushnell, P.R. Kemper, M.T. Bowers, J. Phys. Chem. 99 (1995) 15602.
[7] P.R. Kemper, P. Weis, M.T. Bowers, Int. J. Mass Spectrom. Ion Phys. 160 (1997) 17.
[8] P. Weis, P.R. Kemper, M.T. Bowers, J. Phys. Chem. A 101 (1997) 2809.
[9] J.E. Bushnell, P.R. Kemper, P. Maitre, M.T. Bowers, J. Chem. Phys. 106 (1997) 10153.
[10] P.R. Kemper, P. Weis, M.T. Bowers, Chem. Phys. Lett. 293 (1998) 503.
[11] P.R. Kemper, P. Weis, M.T. Bowers, J. Am. Chem. Soc. 120 (1998) 13494.
[12] M.J. Manard, J.E. Bushnell, S.L. Bernstein, M.T. Bowers, J. Phys. Chem. 106 (2002) 10027.
[13] J.R. Sievers, P.B. Armentrout, J. Phys. Chem. 99 (1995) 8135.
[14] F.A. Khan, D.E. Clemmer, R.H. Schultz, P.B. Armentrout, J. Phys. Chem. 97 (1993) 7978.
[15] R.H. Schultz, K.C. Crellin, P.B. Armentrout, J. Am. Chem. Soc. 113 (1991) 8590.
[16] S. Goebel, C.L. Haynes, F.A. Khan, P.B. Armentrout, J. Am. Chem. Soc. 117 (1995) 6994.
[17] F.A. Khan, D.L. Steele, P.B. Armentrout, J. Phys. Chem. 99 (1995) 7819.
[18] F. Meyer, Y.M. Chen, P.B. Armentrout, J. Am. Chem. Soc. 117 (1995) 4071.
[19] P.A.M. Van Koppen, J. Bushnell, P.R. Kemper, M.T. Bowers, J. Am. Chem. Soc. 117 (1995) 2098.
[20] For a general discussion, see: C.W. Bauschlicher, H. Partridge, S.R. Langhoff, in: B.S. Freiser (Ed.), Organometallic Ion Chemistry, Kluwer Academic, Dordrecht, The Netherlands, 1996.
[21] P.R. Kemper, M.T. Hsu, M.T. Bowers, J. Phys. Chem. 95 (1991) 10600.
[22] J.E. Bushnell, P.R. Kemper, M.T. Bowers, J. Phys. Chem. 98 (1994) 2044.
[23] M. Haruta, Catalysis Today 36 (1997) 153.

[24] G. Mills, M.S. Gordon, H. Metiu, J. Chem. Phys. 118 (2003) 4198.
[25] M. Okumura, Y. Kitazawa, M. Haruta, K. Yamaguchi, Chem. Phys. Lett. 346 (2001) 163.
[26] B.E. Salisbury, W.T. Wallace, R.L. Whetten, Chem. Phys. 262 (2000) 131.
[27] J.H. Lee, K.H. Ervin, J. Phys. Chem. 40 (1994) 10023.
[28] N.R. Walker, R.R. Wright, P.E. Barran, J.N. Murrell, A.J. Stace, J. Am. Chem. Soc. 123 (2001) 4223.
[29] M.B. Knickelbein, Annu. Rev. Phys. Chem. 50 (1999) 79.
[30] P.R. Kemper, M.T. Bowers, J. Am. Soc. Mass Spectrosc. 1 (1990) 197.
[31] (a) P. Hohenberg, W. Kohn, Phys. Rev. B 136 (1964) 864; (b) W. Kohn, L. Sham, J. Phys. Rev. A 140 (1965) 1133.
[32] P.J. Stevens, F.J. Devlin, C.F. Chablowski, M.J. Frisch, J. Phys. Chem. 98 (1994) 11623.
[33] (a) A.K. Becke, J. Chem. Phys. 98 (1993) 5648; (b) A.D. Becke, Phys. Rev. A 38 (1988) 3098.
[34] M.J. Frisch, G.W. Trucks, H.B. Schlegel, G.E. Scuseria, M.A. Robb, J.R. Cheeseman, V.G. Zakrzewski, J.A. Montgomery Jr., R.E. Stratmann, J.C. Burant, S. Dapprich, J.M. Millam, A.D. Daniels, K.N. Kudin, M.C. Strain, O. Farkas, J. Tomasi, V. Barone, M. Cossi, R. Cammi, B. Mennucci, C. Pomelli, C. Adamo, S. Clifford, J. Ochterski, G.A. Petersson, P.Y. Ayala, Q. Cui, K. Morokuma, D.K. Malick, A.D. Rabuck, K. Raghavachari, J.B. Foresman, J. Cioslowski, J.V. Ortiz, A.G. Baboul, B.B. Stefanov, G. Liu, A. Liashenko, P. Piskorz, I. Komaromi, R. Gomperts, R.L. Martin, D.J. Fox, T. Keith, M.A. Al-Laham, C.Y. Peng, A. Nanayakkara, C. Gonzalez, M. Challacombe, P.M.W. Gill, B. Johnson, W. Chen, M.W. Wong, J.L. Andres, C. Gonzalez, M. Head-Gordon, E.S. Replogle, J.A. Pople, Gaussian, Inc., Pittsburgh, PA, 1998.
[35] R. Krishnan, J.S. Binkley, R. Seeger, J.A. Pople, J. Chem. Phys. 72 (1980) 650.
[36] (a) P.J. Hay, W.R. Wadt, J. Chem. Phys. 82 (1985) 270; (b) W.R. Wadt, P.J. Hay, J. Chem. Phys. 82 (1985) 284; (c) P.J. Hay, W.R. Wadt, J. Chem. Phys. 82 (1985) 299.
[37] A.E. Reed, L.A. Curtis, F. Weinhold, Chem. Rev. 88 (1988) 899, and references therein.
[38] A.C. Wahl, Science 151 (1966) 961.